Black Hole Mergers from Star Clusters with Top-heavy Initial Mass Functions

Newlin C. Weatherford[1,2] ⓘ, Giacomo Fragione[1,2] ⓘ, Kyle Kremer[3,4] ⓘ, Sourav Chatterjee[5] ⓘ, Claire S. Ye[1,2] ⓘ,
Carl L. Rodriguez[6] ⓘ, and Frederic A. Rasio[1,2] ⓘ
[1] Center for Interdisciplinary Exploration & Research in Astrophysics (CIERA), Evanston, IL 60202, USA
[2] Department of Physics & Astronomy, Northwestern University, Evanston, IL 60202, USA
[3] TAPIR, California Institute of Technology, Pasadena, CA 91125, USA
[4] The Observatories of the Carnegie Institution for Science, Pasadena, CA 91101, USA
[5] Tata Institute of Fundamental Research, Homi Bhabha Road, Mumbai 400005, India
[6] McWilliams Center for Cosmology, Department of Physics, Carnegie Mellon University, Pittsburgh, PA 15213, USA

Abstract

Recent observations of globular clusters (GCs) provide evidence that the stellar initial mass function (IMF) may not be universal, suggesting specifically that the IMF grows increasingly top-heavy with decreasing metallicity and increasing gas density. Noncanonical IMFs can greatly affect the evolution of GCs, mainly because the high end determines how many black holes (BHs) form. Here we compute a new set of GC models, varying the IMF within observational uncertainties. We find that GCs with top-heavy IMFs lose most of their mass within a few gigayears through stellar winds and tidal stripping. Heating of the cluster through BH mass segregation greatly enhances this process. We show that, as they approach complete dissolution, GCs with top-heavy IMFs can evolve into "dark clusters" consisting of mostly BHs by mass. In addition to producing more BHs, GCs with top-heavy IMFs also produce many more binary BH (BBH) mergers. Even though these clusters are short-lived, mergers of ejected BBHs continue at a rate comparable to, or greater than, what is found for long-lived GCs with canonical IMFs. Therefore, these clusters, though they are no longer visible today, could still contribute significantly to the local BBH merger rate detectable by LIGO/Virgo, especially for sources with higher component masses well into the BH mass gap. We also report that one of our GC models with a top-heavy IMF produces dozens of intermediate-mass black holes (IMBHs) with masses $M > 100 \, M_\odot$, including one with $M > 500 \, M_\odot$. Ultimately, additional gravitational wave observations will provide strong constraints on the stellar IMF in old GCs and the formation of IMBHs at high redshift.

Unified Astronomy Thesaurus concepts: Initial mass function (796); Stellar mass black holes (1611); Globular star clusters (656); Stellar dynamics (1596); N-body simulations (1083); Gravitational wave sources (677)

1. Introduction

Among the densest environments in the universe, globular clusters (GCs) are ideal laboratories to investigate the importance of stellar dynamics in forming and evolving compact objects and compact binaries (see, e.g., Heggie & Hut 2003). Frequent dynamical encounters between cluster members are fundamental in creating and explaining the existence of a number of exotic populations, such as X-ray binaries (e.g., Clark 1975; Verbunt et al. 1984; Giesler et al. 2018; Kremer et al. 2018), radio pulsars (e.g., Lyne et al. 1987; Sigurdsson & Phinney 1995; Ivanova et al. 2008; Ye et al. 2019), and gravitational wave (GW) sources (e.g., Rodriguez et al. 2015; Askar et al. 2017; Banerjee 2017; Fragione & Kocsis 2018; Kremer et al. 2019).

Many results of GC modeling rely on the assumption that the stellar initial mass function (IMF) has the form of a canonical Kroupa (2001) IMF. Observations, however, suggest the IMF may not be universal. For example, Milky Way GCs with low central densities appear deficient in low-mass stars (De Marchi et al. 2007), while GCs in the Andromeda galaxy exhibit a trend between metallicity and mass-to-light ratio that only a noncanonical, top-heavy IMF could explain (Haghi et al. 2017). Ultracompact dwarf galaxies have large dynamical mass-to-light ratios and appear to contain an overabundance of LMXB sources (Dabringhausen et al. 2009). Our Galactic center provides an extreme example of a noncanonical IMF; stars formed there in the past few megayears have masses

consistent with a top-heavy mass function (Bartko et al. 2010). All these observations can be explained if the stellar IMF becomes increasingly top-heavy with decreasing metallicity and increasing gas density of the pre-GC cloud (Marks et al. 2012). This is theoretically expected given the Jeans mass instability in molecular clouds (Larson 1998) and self-regulation of accretion onto forming stars (Adams & Fatuzzo 1996; Adams & Laughlin 1996). Metallicity plays a decisive role by regulating line-emission cooling in the collapsing gas cloud and radiation pressure against stellar accretion (De Marchi et al. 2017).

The IMF has long been known to strongly impact the dynamical evolution and survival of GCs. Already Chernoff & Weinberg (1990) found enhanced mass loss rates in cluster models with flatter IMFs, due to increased winds from high-mass stars and faster halo expansion and evaporation. More recent results show that GC models with top-heavy IMFs dissolve much faster than models with canonical IMFs (Chatterjee et al. 2017; Giersz et al. 2019). In particular, clusters with top-heavy IMFs produce more numerous and more massive black holes (BHs). Crucially, this promotes the BH-burning process, in which strong dynamical encounters with BHs provide energy to stellar populations, inflating the cluster halo (Mackey et al. 2007, 2008; Breen & Heggie 2013; Kremer et al. 2020a). Taken to an extreme by a top-heavy IMF, this mechanism will force rapid and unstable evaporation through the tidal boundary and early cluster dissolution (Giersz et al. 2019).

The impact on cluster evolution of varying BH abundance has recently been further analyzed via a combination of analytical calculations and *N*-body simulations (Breen & Heggie 2013; Wang 2020). However, these studies only consider idealized star clusters with two components (stars and BHs) and no stellar evolution, which plays a crucial role in cluster disruption (e.g., Chernoff & Weinberg 1990). Apart from the few models with noncanonical IMFs examined by Chatterjee et al. (2017) and Giersz et al. (2019), there is no systematic study of the IMF's influence on BH populations generated via stellar evolution. In this Letter, we extend the grid of cluster models in the CMC Cluster Catalog (Kremer et al. 2020b), focusing on the role of a varying IMF. In particular, we study how noncanonical IMFs shape the evolution of GCs, their BH populations, and the number of dynamically produced BBH mergers.

The Letter is organized as follows. In Section 2, we describe the parameters of the numerical models we evolve. In Section 3, we analyze the structural evolution of clusters and describe the properties of their black hole populations, including BBH mergers. Finally, in Section 4, we discuss the implications of our findings and lay out our conclusions.

2. Cluster Models

To evolve our cluster models, we use CMC (Cluster Monte Carlo), a Hénon-type Monte Carlo code that includes the newest prescriptions for wind-driven mass loss, compact object formation, and pulsational-pair instabilities (see Hénon 1971a, 1971b; Joshi et al. 2000, 2001; Fregeau et al. 2003; Chatterjee et al. 2010, 2013; Pattabiraman et al. 2013; Rodriguez et al. 2015; Kremer et al. 2020b, and references therein).

We generate 15 independent cluster simulations varying the initial number of particles (single stars plus binaries) N_i and initial total mass M_i, with uniform initial cluster virial radius ($r_v = 1$ pc), metallicity ($Z = 0.1\,Z_\odot$), and Galactocentric distance[7] ($R_{gc} = 8$ kpc). These choices of r_v, R_{gc}, and Z are known to result in models that closely match typical Milky Way GCs when using a canonical IMF (Kremer et al. 2020b).

We assume that all models are initially described by a King profile with concentration $W_0 = 5$ (King 1962). Primary stellar masses are sampled from the Kroupa (2001) multicomponent power-law IMF,

$$\xi(m) \propto \begin{cases} m^{-1.3} & 0.08 \leqslant m/M_\odot \leqslant 0.5 \\ m^{-2.3} & 0.5 \leqslant m/M_\odot \leqslant 1.0 \\ m^{-\alpha_3} & 1.0 \leqslant m/M_\odot \leqslant 150.0. \end{cases} \quad (1)$$

We choose three different values for $\alpha_3 = (1.6, 2.3, 3.0)$, corresponding to the 95% confidence interval around the canonical value, $\alpha_3 = 2.3$ (Kroupa 2001). We fix the primordial stellar binary fraction to $f_b = 5\%$ and draw secondary masses from a uniform distribution in mass ratio (e.g., Duquennoy & Mayor 1991). Binary orbital periods are sampled from a log-uniform distribution, with orbital separations ranging from near contact to the hard/soft boundary, while binary eccentricities are thermal (e.g., Heggie 1975). For details on stellar evolution in CMC, see Kremer et al. (2020b). We compute GW recoil kicks for BH merger products

following the methods described in Rodriguez et al. (2019) and references therein. We assume all BHs have zero natal spin while BH merger products are assigned new spins of $\sim$0.7 (e.g., Berti et al. 2007; Tichy & Marronetti 2008; Lousto et al. 2010), which are then taken into account if they merge again.

Table 1 summarizes the model parameters considered in our work. Each simulation evolves to a final time $T_H \approx 14$ Gyr, unless the cluster disrupts. In these cases, which occur only for our models with $\alpha_3 = 1.6$, simulation terminates once there are fewer than 300 particles per CPU, the default particle count used to compute local densities throughout the cluster. This typically corresponds to a few $\times 10^4$ stars in the GC, beyond the point where the assumptions of the Monte Carlo method—namely spherical symmetry and a relaxation timescale longer than the dynamical timescale—start to break down (Chatterjee et al. 2017). However, the exact cutoff point in the simulation does not affect the general evolutionary trends of the dissolution process. Further accurate evolution of the remaining "dark star cluster" would require a switch to direct *N*-body methods (e.g., Banerjee & Kroupa 2011).

3. Results

In this section, we discuss how different IMFs affect the evolution of the cluster mass, size, and BH population. We do not find significant qualitative differences between the cases where we keep the initial number of particles constant (models 1–3, 7–9, and 10–12 in Table 1) or the initial total mass constant (models 4–9 and 13–15).

3.1. Cluster Evolution

Variations in the high end of the IMF can dramatically affect cluster evolution and survival, especially by setting the number of BHs that are formed and retained, determining the degree to which BH-burning regulates the cluster's energy reservoir (Chatterjee et al. 2017). In this process, BHs quickly mass-segregate into the cluster core on a subgigayear timescale, forming a central BH population that undergoes frequent phases of core collapse and re-expansion (Morscher et al. 2015). During these events, the BHs mix with the rest of the cluster and provide energy to passing stars in scattering interactions (Breen & Heggie 2013). Cumulatively, these interactions inflate the cluster halo and force faster evaporation through the tidal boundary (Chatterjee et al. 2017; Giersz et al. 2019; Wang 2020).

In Figure 1, we show the evolution of the total mass (top left panel) for star clusters with different N_i and α_3. Clusters evolve very differently depending on the choice of α_3. The models with $\alpha_3 = 2.3$ and 3 survive until T_H, while the models with $\alpha_3 = 1.6$ appear to disrupt at about $t \sim 1$ Gyr with faster disruption occurring for smaller N_i.[8] The different fates of the cluster models are understandable given the mechanisms that power cluster mass loss at different epochs:

1. Initially, mass is lost primarily via stellar winds from massive stars (e.g., Chernoff & Weinberg 1990). This relatively quiet first phase is visible early in the top left panel of Figure 1, terminating around $t \approx 3$ Myr.

---

[8] While these models may not survive with significant mass beyond a few gigayears, models with larger N_i, larger Galactocentric distance, and/or smaller virial radius could feasibly survive much longer.

Table 1
Model Initial Conditions and Data on Cumulative BH Formation and BBH Mergers

	α_3	N_i (10^5)	M_i $(10^5\ M_\odot)$	N_{BH}	BBH mergers $N_{BBH}^{(merg)}$	$N_{BBH,ejected}^{(merg)}$	$N_{BBH,gap,coll}^{(merg)}$	$N_{BBH,gap,2G+}^{(merg)}$	$N_{BBH}^{(merg)}(z<1)$
1	1.6	4	8.5	11263	95	58	1	7	7
2	1.6	8	17.0	22539	222	132	7	26	19
3	1.6	16	34.2	45358	434	195	32	83	14
4	1.6	1.1	2.4	3224	20	15	0	2	0
5	1.6	2.3	4.8	6319	57	42	1	3	5
6	1.6	4.5	9.6	12764	111	73	5	10	11
7	2.3	4	2.4	1114	38	17	1	3	5
8	2.3	8	4.8	2252	91	36	0	9	13
9	2.3	16	9.7	4518	233	106	1	23	42
10	3.0	4	1.6	113	6	0	0	1	0
11	3.0	8	3.3	247	9	3	0	1	2
12	3.0	16	6.6	499	32	6	1	2	1
13	3.0	5.9	2.4	188	9	1	0	1	0
14	3.0	11.8	4.8	341	28	3	1	1	2
15	3.0	23.6	9.7	744	71	9	2	5	7

Note. The BH and BBH merger totals are cumulative between $0 \leqslant t \leqslant 13$ Gyr. From left to right, the columns are upper-IMF slope α_3, initial number of particles N_i, initial mass M_i, total BHs formed N_{BH}, total BBH mergers $N_{BBH}^{(merg)}$, ejected BBH mergers $N_{BBH,ejected}^{(merg)}$, BBH mergers with a "mass-gap" BH component $(M_{BH} > 40.5 M_\odot)$ formed via stellar collisions $N_{BBH,gap,coll}^{(merg)}$, multiple-generation BBH mergers with a mass-gap BH component $N_{BBH,gap,2G+}^{(merg)}$, and total BBH mergers at redshifts $z < 1$, $N_{BBH}^{(merg)}(z\backslash lt1)$, assuming that all GCs were born 13 Gyr ago. Note that the BBH merger totals in the last five columns for models 1-6 are all lower limits since we do not consider mergers resulting from dynamics in "dark clusters" (see Section 3.3).

2. The second phase of mass loss, extending from 3 Myr $\lesssim t \lesssim$ 60 Myr, is driven primarily by Type II supernovae (SNe) accompanying compact object formation. This phase most clearly depends on the choice of α_3. For $\alpha_3 = 3$, SNe-driven mass loss from few massive stars is negligible compared to ongoing stellar wind mass loss among the far more numerous low-mass stars. For $\alpha_3 = 1.6$, however, the SNe-driven mass loss phase is nearly catastrophic, causing the cluster to lose close to half its original mass by the time compact object formation slows ($t \approx 60$ Myr). Ejections of lighter compact objects due to natal kicks also contribute to mass loss in this phase starting at $t \approx 6$ Myr, causing a plateau in N_{BH} (top right panel).

3. A "third phase" of mass loss begins at the end of rapid compact object formation. Really just a return of the first phase, this period of mass loss is once again dominated by stellar winds, this time from lower-mass stars. For the models, where $\alpha_3 = 2.3$ or 3, stellar winds continue to account for most of the mass loss until about 6 Gyr. The wind-dominated mass loss phase ends much earlier for the $\alpha_3 = 1.6$ models—around $t \approx 200$ Myr.

4. The fourth and final phase of mass loss is driven by evaporation through the tidal boundary. This phase depends strongly on the IMF due to its influence on the number of BHs formed, and thereby the degree to which BH-burning inflates the halo. In the case of extreme BH-burning, the cluster quickly expands to fill its Roche lobe within the assumed Galactic potential and starts to tidally disrupt, as seen in the models with $\alpha_3 = 1.6$. Note that similar accelerating mass loss is also seen at late times in the models with $\alpha_3 = 3$. In these models, however, the runaway process of halo evaporation and tidal contraction is not stimulated by extreme BH-burning. Instead, these top-light, low-mass models simply start out with much smaller tidal radii. Hence they see significant evaporation

rates relatively quickly compared to canonical models ($\alpha_3 = 2.3$), despite forming far fewer BHs.

The evolution of the half-mass–radius r_h (bottom left panel, Figure 1) also reflects this general picture. In all models, r_h expands as a consequence of stellar mass loss. Enhanced BH-burning in models with $\alpha_3 = 1.6$ drives faster cluster expansion such that these models overflow their Roche lobes after a few hundred megayears. Due to more energetic BH-burning, these clusters lose about 80% of their mass by $t \sim 1$ Gyr. Models with $\alpha_3 = 3$ do not exhibit rapid expansion, evolving more gradually as a result of reduced massive star formation and the lack of a significant central BH population.

3.2. Black Hole Population

In the top right panel of Figure 1, we show the evolution of the number of BHs N_{BH}. Clusters with top-heavy IMFs produce more high-mass stars and thereby more BHs. As described above, natal kicks start to eject newly formed BHs after $t \approx 6$ Myr, causing N_{BH} to plateau for each model. At this point, we find that N_{BH} in models with $\alpha_3 = 1.6$ is $\sim$10 times higher than in models with $\alpha_3 = 2.3$ and $\sim$100 times higher than in models with $\alpha_3 = 3$ (see also the cumulative number of BHs formed in column 4 of Table 1). During this phase of roughly constant N_{BH}, dynamical friction causes BHs to segregate to the cluster center. This phase's duration depends on α_3 since clusters with top-heavy IMFs have higher average stellar mass and correspondingly longer segregation timescales. Once the BHs have segregated to the core, they are gradually ejected via strong dynamical encounters.

In the bottom right panel of Figure 1, we also show the evolution of the fractional number of BHs N_{BH}/N. In models with $\alpha_3 = 2.3$ or 3, N_{BH}/N decreases in time as strong encounters preferentially eject massive objects (e.g., BHs) from the cluster core. In models with $\alpha_3 = 1.6$, however, N_{BH}/N increases in time due to earlier tidal evaporation. By the
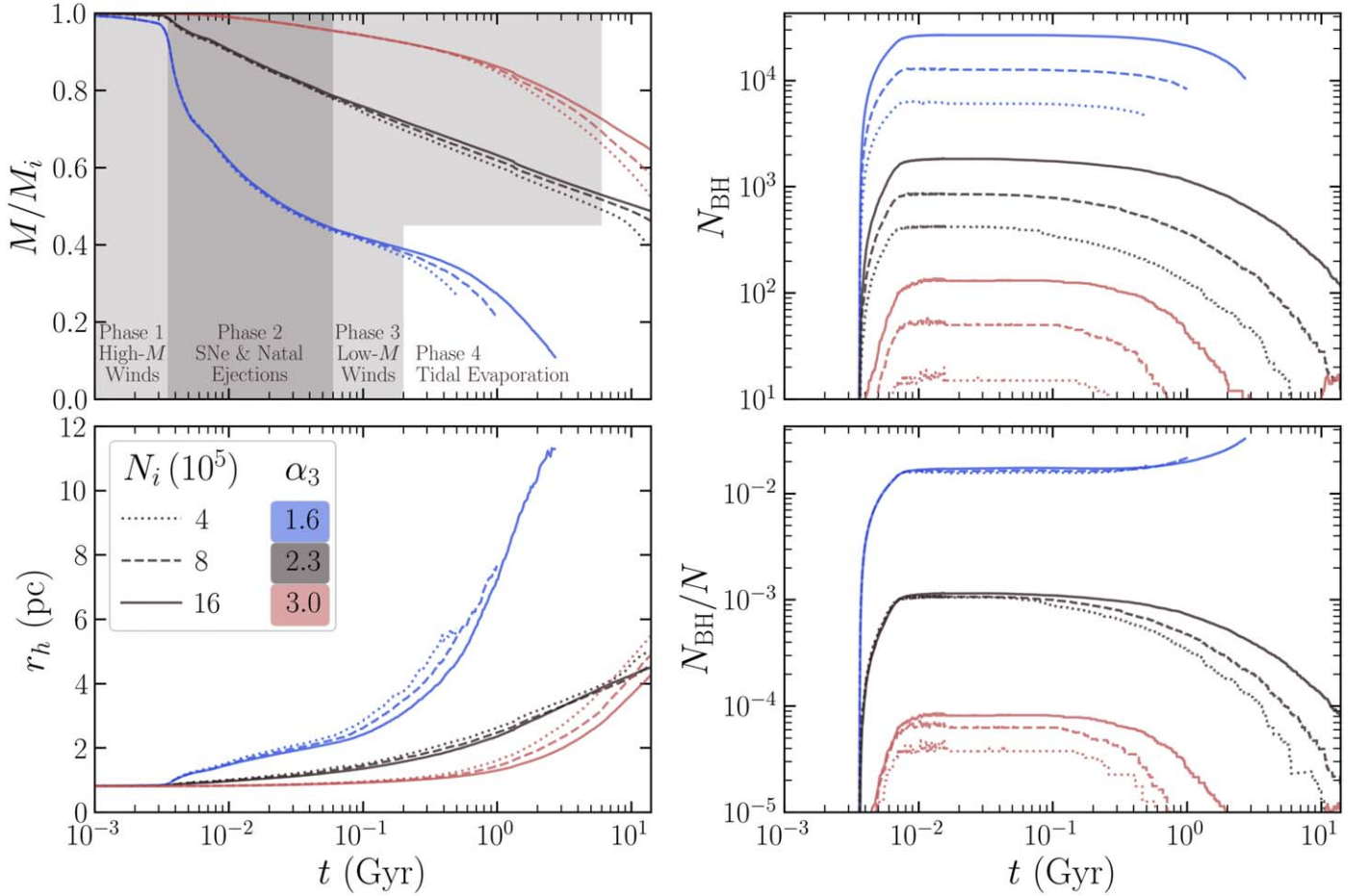
Figure 1. Evolution of the total mass (top left), half-mass–radius r_h (bottom left), number of BHs N_{BH} (top right), and fractional number of BHs N_{BH}/N (bottom right) for cluster models with different values of α_3 (blue 1.6, black 2.3, and red 3.0). Different line styles represent different initial numbers of particles (dotted 4×10^5, dashed 8×10^5, and solid 1.6×10^6). The simulations terminate at $T_H = 14$ Gyr, except for $\alpha_3 = 1.6$, where we cut off the plot just before r_h starts to drop sharply (around this point, assumptions in our Monte Carlo methods stop being valid; see the text). In the top left panel, the four mass loss phases discussed in the text are highlighted via shaded intervals and the dominant mass loss mechanisms indicated. The bifurcation of the third phase is due to decreased duration of this phase for $\alpha_3 = 1.6$.

moment these clusters retain only ∼20% of their original mass, $N_{BH}/N \approx 3\%–4\%$, corresponding to a significant fraction of cluster mass (up to 75% by the time r_h peaks). Note that the number and mass fraction of BHs at late times depends on the cluster dissolution process beyond this point, which our Monte Carlo methods are not designed to address. It is nevertheless clear that clusters with top-heavy IMFs can evolve through a "dark cluster" stage during which their total mass is dominated by BHs (e.g., Banerjee & Kroupa 2011).

Regardless of age, individual BHs are only directly detectable if they reside in binaries, either via detection of GWs from BBH mergers or through the presence of non-BH (nBH) companions. While dense star clusters are expected to be efficient factories of BBH and BHnBH binaries, their numbers typically remain small as their dynamical assembly competes with their disruption and ejection (e.g., Downing et al. 2010, 2011; Morscher et al. 2015; Kremer et al. 2018). However, the choice of IMF greatly impacts BH binary formation.

In Figure 2, we plot the evolution of the number of BBHs N_{BBH}. Clusters with top-heavy IMFs produce more BBHs via enhanced formation of high-mass stars and BHs. N_{BBH} plateaus a little later than N_{BH} (top right panel, Figure 1), a delay reflecting the dynamical assembly of BBHs. An equilibrium

between N_{BBH} and N_{BH} is apparent during this plateau, with the order of one BBH for every 100 bound BHs in the cluster. Subsequently, N_{BBH} decreases more rapidly for clusters with higher N_{BH}, as evident by the slope past the plateau. This is unsurprising since BH-burning, enhanced for clusters with higher N_{BH}, is characterized by periodic collapse and re-expansion of the central BH population, a process that disrupts and ejects many BBHs (Morscher et al. 2015; Chatterjee et al. 2017).

3.3. BBH Merger Rates

We report in Table 1, column 5, the cumulative numbers of BBH mergers $N_{BBH}^{(merg)}$ in each model through 13 Gyr. It is readily apparent that each reduction in α_3 generally increases $N_{BBH}^{(merg)}$, with some nuance introduced depending on which values of α_3 are compared and whether N_i or M_i is held constant in the comparison. Most notably, $N_{BBH}^{(merg)}$ in short-lived clusters with $\alpha_3 = 1.6$ is comparable to or greater than the number in their longer-lived cousins with $\alpha_3 = 3$. This is largely due to the sheer number of merging BBHs they eject (Table 1, column 6).

Even though clusters with top-heavy IMFs rapidly dissolve, the large number of merging BBHs they eject suggests they
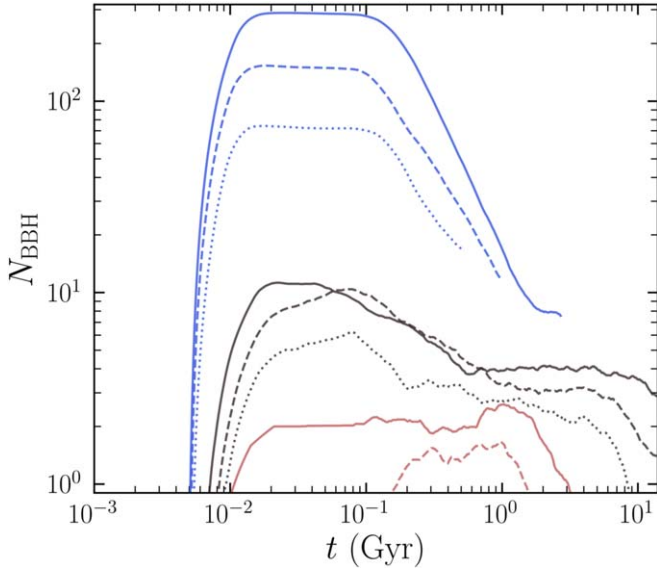
Figure 2. Evolution of the number of binary black holes $N_{\rm BBH}$ bound to the star clusters with different values of α_3 (blue 1.6, black 2.3, and red 3.0) and different initial number of particles (N_i). Different line styles represent different N_i, as in Figure 1. Since BBHs continuously form and disrupt in central scattering interactions, we apply a rolling average over every 10^4 time-steps to smooth the curves at low $N_{\rm BBH}$.

Figure 3. Cumulative binary black hole mergers with respect to redshift (and time) for star clusters with different values of α_3 (blue 1.6, black 2.3, red 3.0) and different initial number of particles (N_i). Different line styles represent different N_i, as in Figure 1. All model GCs were assumed to be born 13 Gyr ago and appropriate redshifts were then computed using `Astropy`'s (Astropy Collaboration et al. 2013) cosmology calculator under the flat ΛCDM model with $H_0 = 69.6\,{\rm km/s/Mpc}$ and $\Omega_{\rm matter} = 0.286$ (see, e.g., Bennett et al. 2014). Values for $\alpha_3 = 1.6$ are lower limits (see Section 3.3).

could contribute significantly to the total BBH merger rate in the local universe. Indeed, we show in Figure 3 that the distribution of BBH mergers across redshift z is roughly comparable between the models with $\alpha_3 = 1.6$ and 2.3, even for $z < 1$. The number of BBH mergers in each model at $z < 1$ is listed in column 9 of Table 1: a total of 40 across models 1–3 with $\alpha_3 = 1.6$ vs. 60 across models 7–9 with $\alpha_3 = 2.3$. This comparison is quite conservative since the merger counts for the models with $\alpha_3 = 1.6$ are lower limits. First, we only consider BBHs ejected prior to the simulation's end, ignoring the potentially substantial contribution to the $z < 1$ merger rate from the large number of bound BHs left in the "dark phase" of these clusters' evolution. Many of these BHs could merge after ejection as binaries. Second, to compute redshift we assume the clusters were uniformly born 13 Gyr ago, ignoring entirely the possibility that clusters with top-heavy IMFs may be born more recently (El-Badry et al. 2019). It is therefore plausible that clusters born with top-heavy IMFs could still contribute significantly to the local BBH merger rate even if they are dissolved by the present day (Fragione & Kocsis 2018).

Since the above comparisons of $z < 1$ merger counts are model-dependent, it is useful to more generally estimate the BBH merger rate expected in clusters with top-heavy IMFs. We do so using the total number of BBH mergers from each model (which are still lower limits in the case of $\alpha_3 = 1.6$). The rate due to clusters with $\alpha_3 = x$ at a given redshift z can be approximated as $\Gamma_x(z) \approx \langle N_{\rm BBH}^{\rm (merg)}/M_i \rangle \rho_{\rm SF}(z) f_{\rm SF} f_x$. Here, $\langle N_{\rm BBH}^{\rm (merg)}/M_i \rangle$ is the mean number of BBH mergers per initial cluster mass, $\rho_{\rm SF}$ is the cosmological density of the star formation rate, $f_{\rm SF}$ is the fraction of the star formation rate assumed to occur in star clusters, and f_x is the fraction of clusters born with $\alpha_3 \approx x$. To mitigate uncertainties in the latter three terms, we simply compute $\langle N_{\rm BBH}^{\rm (merg)}/M_i \rangle$ for each value of α_3 and express the estimated merger rates from clusters with noncanonical IMFs as ratios with respect to the better-studied rates from clusters with canonical IMFs.
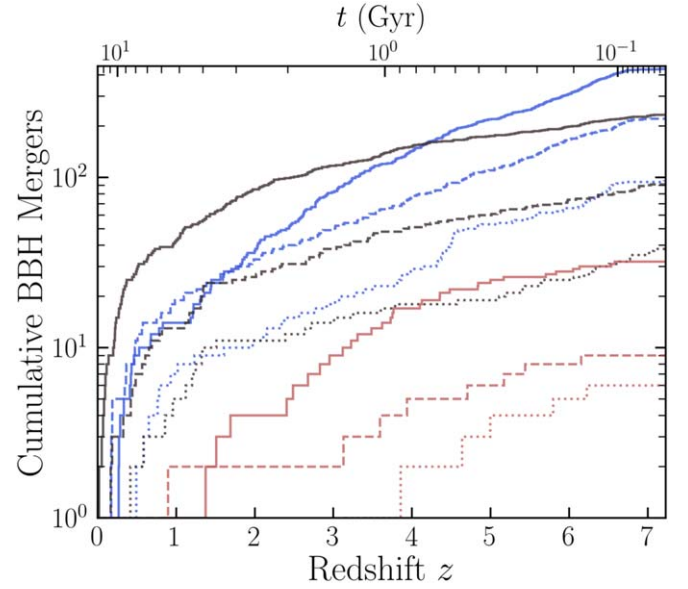
To compute $\langle N_{\rm BBH}^{\rm (merg)}/M_i \rangle$ for each α_3, we extract the functional dependence of $N_{\rm BBH}^{\rm (merg)}$ on M_i from columns 3 and 5 of Table 1. Though the number of BBH mergers per cluster scales roughly linearly with the present-day cluster mass, at least in clusters with canonical IMFs (e.g., Rodriguez et al. 2015; Kremer et al. 2020b), we find a more general power law of the form $N_{\rm BBH}^{\rm (merg)} = a(M_i)^b$ fits the data slightly better given χ^2 goodness-of-fit tests. Specifically,

$$N_{\rm BBH}^{\rm (merg)} \begin{cases} \geqslant (9.5 \pm 1.0)\left(\frac{M_i}{10^5 {\rm M_\odot}}\right)^{1.09 \pm 0.04} & \alpha_3 = 1.6 \\[2mm] = (11.8 \pm 0.5)\left(\frac{M_i}{10^5 {\rm M_\odot}}\right)^{1.31 \pm 0.02} & \alpha_3 = 2.3 \\[2mm] = (1.9 \pm 0.7)\left(\frac{M_i}{10^5 {\rm M_\odot}}\right)^{1.6 \pm 0.2} & \alpha_3 = 3.0, \end{cases} \quad (2)$$

where the 1σ uncertainties on the fit parameters are computed assuming Poisson uncertainties on $N_{\rm BBH}^{\rm (merg)}$ and the $\geqslant$ symbol indicates a lower limit for top-heavy IMFs.

Assuming the distribution of GC birth masses takes the form $dN_{\rm cluster}/dM_i \propto M_i^{-2}$ (Lada & Lada 2003), then

$$\left\langle \frac{N_{\rm BBH}^{\rm (merg)}}{M_i} \right\rangle = \frac{a}{(10^5 {\rm M_\odot})^b} \frac{\int_{M_L}^{M_H} M_i^{b-3} dM_i}{\int_{M_L}^{M_H} M_i^{-2} dM_i}$$

$$= \begin{cases} \frac{a M_H \ln(M_H/M_L)}{(10^5 {\rm M_\odot})^2 (M_H/M_L - 1)} & b = 2 \\[3mm] \frac{a M_L^{b-1}}{(2-b)(10^5 {\rm M_\odot})^b}\left[\frac{1 - (M_L/M_H)^{2-b}}{1 - M_L/M_H}\right] & b \neq 2, \end{cases} \quad (3)$$

where M_L and M_H are the lower and upper limits of the mass function for clusters capable of producing BBH mergers. Both bounds are somewhat arbitrary, but the lower bound has a

greater impact on the merger rate calculation since the integrands in Equation (3) scale inversely with M_i. To avoid extrapolating our fit to cluster masses that rarely produce BBHs, we set the lower bound for each α_3 as the M_i that produces an average of two stars with $M > 25$ $M_\odot$, given the assumed IMF. This is roughly the minimum cluster mass needed to produce a single BBH merger since most progenitors with $M > 25$ $M_\odot$ will collapse to a BH. Under this definition, $M_L/(100 M_\odot) \approx (2, 9, 80)$ for $\alpha_3 = (1.6, 2.3, 3)$, respectively. Although the maximum cluster mass could vary with α_3 in principle, observations do not well-constrain this value, so we naïvely set the upper bound for all α_3 to be $M_H = 10^7 M_\odot$ (Harris et al. 2014). With these assumptions, we find that $\langle N_{\mathrm{BBH}}^{(\mathrm{merg})}/M_i \rangle \approx (59, 40, 10)/(10^6\ M_\odot)$, respectively. The rates for GCs with $\alpha_3 = 1.6$ and 3, relative to the rates in canonical GCs with $\alpha_3 = 2.3$, are then roughly given by

$$\frac{\Gamma_{1.6}}{\Gamma_{2.3}} \gtrsim 1.5 \frac{f_{\mathrm{GC},1.6}}{f_{\mathrm{GC},2.3}}, \qquad \frac{\Gamma_{3.0}}{\Gamma_{2.3}} \approx 0.25 \frac{f_{\mathrm{GC},3.0}}{f_{\mathrm{GC},2.3}}. \qquad (4)$$

Note again that the above ratio for clusters with $\alpha_3 = 1.6$ is a lower limit. Both ratios are also very approximate since we neither consider interdependence of M_i and α_3 nor any cumulative dependency of these ratios on the choices of initial parameters, such as virial radius, Galactocentric distance, metallicity, and binary fraction. Furthermore, f_x is notoriously uncertain and could depend on redshift, metallicity, and time of birth. Nevertheless, these estimates qualitatively suggest that if $f_{1.6} > f_{2.3} \gtrsim f_{3.0}$, then the contribution to the cosmological BBH merger rate from clusters could be a bit higher than currently estimated (e.g., by Kremer et al. 2020b). In turn, if $f_{3.0} > f_{2.3} \gtrsim f_{1.6}$, then those rate estimates could be too high already. Overall, uncertainties in the IMF may contribute about an order of magnitude to the uncertainty on the dynamical BBH merger rate (see also Chatterjee et al. 2017).

Finally, it is worth commenting briefly on black hole–neutron star (BH-NS) and binary neutron star (BNS) mergers. In clusters that retain a BH population, NSs are pushed out of the dense, BH-filled core due to mass segregation. Hence the merger likelihood is significantly smaller for BH-NS and BNS mergers than for BBH mergers in most GCs (Ye et al. 2020). It is therefore unsurprising that all our models produce insignificant numbers of BH-NS and BNS mergers. While our models with $\alpha_3 = 3$—and therefore very few formed BHs—do exhibit about four times more frequent binary NS mergers than the models with $\alpha_3 = 2.3$, the numbers are still far too low to account for the LIGO/Virgo estimated rates (Fragione & Banerjee 2020; Ye et al. 2020).

3.4. BH and BBH Merger Masses

The average stellar mass is higher in clusters with top-heavy IMFs and lower in clusters with top-light IMFs. So, it is unsurprising that the average masses of BHs, BBH merger components, and BBH merger products in our models all increase with decreasing α_3. Averaging across all our models for each α_3 value, we find a mean BH mass at formation of $(16, 12, 9) M_\odot$ for $\alpha_3 = (1.6, 2.3, 3)$, respectively. The corresponding mean masses for BBH merger components and merger products are $(38, 26, 21) M_\odot$ and $(74, 51, 40) M_\odot$. This trend is further exhibited in Figure 4 showing the mass distribution of BBH merger components. The vertical jump in the distributions at $M = 40.5$ $M_\odot$ is due to the pile-up at the start of the "mass gap" of BHs formed from massive stars via
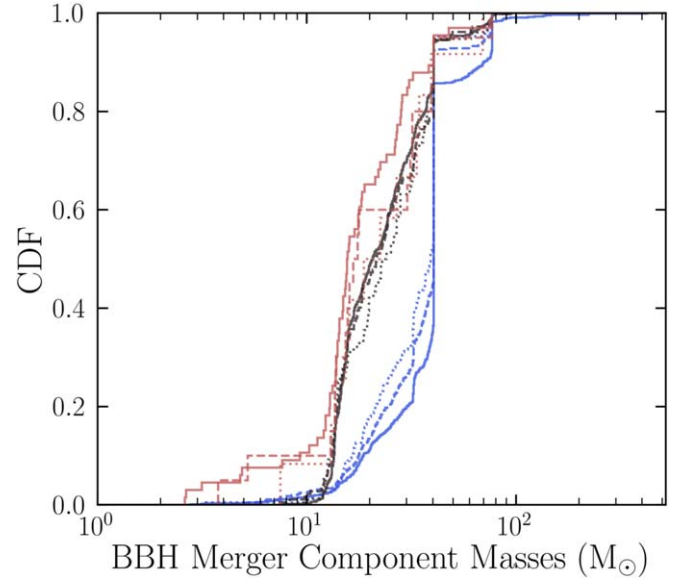

Figure 4. Cumulative density functions (CDFs) of the component masses for binary black hole mergers in star clusters with different values of α_3 (blue 1.6, black 2.3, and red 3.0) and different initial number of particles (N_i). Different line styles represent different N_i, as in Figure 1.

pulsational pair-instability supernovae (PPISNe). CMC assumes this gap begins at $M > 40.5$ $M_\odot$ (for details, see Belczynski et al. 2016), extending to around $120\ M_\odot$. Hence, the first vertical jump indicates that clusters with top-heavy IMFs form significantly more BHs via PPISNe than clusters with canonical IMFs. A second, smaller jump in the distributions for top-heavy IMFs at $M \approx 77\ M_\odot$ arises from second-generation mergers with a component produced in an earlier merger between two such PPISNe-generated BHs.

The anticorrelation between the average mass of BBH merger components and α_3 arises for three reasons. First, clusters with top-heavy IMFs produce higher-mass stars, increasing not only the number of BHs formed, but also their average mass. Second, for initial N held constant, clusters with top-heavy IMFs also have greater total mass and higher collision rates in their densely populated cores. This collision rate enhancement is obvious in Table 1, column 7, listing the number of mass gap BBH merger components formed from the stellar product of collisions (e.g., Di Carlo et al. 2020; Kremer et al. 2020c). While the column only lists collisionally formed merger components in the mass gap, the overall collision rate scales similarly with decreasing α_3. Finally, the increased merger frequency in clusters with top-heavy IMFs itself increases the average mass of the components by increasing the chances that they will have already experienced a merger (e.g., Fragione et al. 2020a, 2020b; Rodriguez et al. 2020).

Indeed, the cumulative number of second-generation or higher (2G+) BBH mergers is also enhanced in clusters with top-heavy IMFs, as seen in Table 1, column 8, listing the number of 2G+ mergers with a component in the mass gap. For clusters with top-heavy IMFs, this is identical to the total number of 2G+ BBH mergers, though 2G+ mergers with neither component in the mass gap are common for higher α_3. Overall, 2G+ merger totals roughly double with each decrease in α_3 from 3 to 2.3 to 1.6, while the numbers of 2G+ mergers with a mass gap component roughly quadruple.

Though we find no trend between initial N and merger component or product mass for $\alpha_3 = 2.3$ or 3, there is a clear

correlation for $\alpha_3 = 1.6$. In this case, for $N_i = (4, 8, 16) \times 10^5$, the average BBH merger product mass is $(54, 62, 79)M_\odot$, respectively. This rise is in part due to 2G+ mergers, which account for (7%, 12%, and 18%) of the BBH mergers in these respective models. In general, we find that clusters with top-heavy IMFs and high initial N are especially good at efficiently producing many 2G+ mergers and many BHs in the mass gap.

The increased collision and 2G+ merger rates in clusters with top-heavy IMFs can also result in the formation of "intermediate-mass" BHs (IMBHs), which we define as BHs with masses exceeding $100\,M_\odot$. In particular, our highest-N model with $\alpha_3 = 1.6$ (model 3 in Table 1) produces 46 IMBHs, including one with mass $M = 537\,M_\odot$. This particular IMBH formed in the merger of a $122\,M_\odot$ IMBH with a $426\,M_\odot$ IMBH, which itself formed in the merger of two IMBHs with $M \approx 200\,M_\odot$. While we intend to explore IMBH formation in GCs with top-heavy IMFs more thoroughly in future work, we for now direct the reader's attention to our collaboration's recent study on IMBH formation in GCs (González et al. 2020).

4. Discussion and Conclusions

Observations provide evidence that the stellar IMF may not be universal. A noncanonical IMF can greatly affect a star cluster's dynamical evolution, especially since its high end determines how many BHs form within, regulating the cluster's energy budget and dynamical clock (Breen & Heggie 2013; Chatterjee et al. 2017; Kremer et al. 2020a; Wang 2020). In this Letter, we have extended the CMC Cluster Catalog (Kremer et al. 2020b) to examine how a varying IMF affects the evolution of star clusters and their BH populations.

We have shown that massive star clusters with top-heavy IMFs (low α_3) are likely to lose most of their mass within a few gigayears, assuming they have low-to-average mass and Galactocentric distance for typical Milky Way GCs. The rapid mass loss during dissolution occurs in stages, first driven by stellar winds and dynamical ejections, then by evaporation of the halo through the tidal boundary. Extensive BH-burning enhances the latter stage in clusters with top-heavy IMFs, which produce many BHs. Such clusters evolve through a point where they consist mostly of BHs by mass (and up to at least 3% by number).[9] Further study with direct N-body methods (e.g., Banerjee & Kroupa 2011) is required to fully understand the evolution of these clusters. Initializing direct N-body simulations with the pre-dissolution states of CMC models could be especially useful in such an evaluation across the full cluster mass distribution.

We note that the processes described above are also affected by the choices of initial cluster metallicity and natal kick distribution (Chatterjee et al. 2017). BHs in metal-rich clusters have lower mass and do not inject as much energy into the BH-burning process as BHs in metal-poor clusters. Thus, metal-rich clusters typically have higher densities and dispersion velocities, therefore processing the BH population on shorter timescales and disrupting more binaries. Meanwhile, high natal kicks will eject most BHs from the cluster during formation. In such a case, BHs and BBHs are expected to be small in number

regardless of the IMF. Top-heavy clusters with higher natal kicks also live longer; while they experience less tidal mass loss driven by BH-burning, these clusters lose even more mass due to kick-driven dynamical ejections of BHs (Chatterjee et al. 2017). For a recent study of top-heavy cluster evolution featuring different natal kick assumptions, see Haghi et al. (2020, published during the review of this paper), who examine lower-mass clusters with direct N-body simulations incorporating gas expulsion physics. Notably, they find that top-heavy clusters, albeit drastically reduced in mass, may well survive to the present day if born with masses above $M_i \gtrsim 7 \times 10^5\,M_\odot$. For times not too close to disruption, where CMC's assumptions start to be challenged (see Section 2), our results are encouragingly compatible with those of Haghi et al. (2020).

Regardless of their long-term evolution and stability, we have also shown that clusters with top-heavy IMFs—and correspondingly high BH production—may contribute significantly to the present-day binary BH merger rate. Even though these clusters rapidly lose most of their mass within a few gigayears, mergers from ejected BBHs continue to contribute at later times (Fragione & Kocsis 2018), at rates comparable to or greater than those for clusters with canonical Kroupa IMFs. The rate of second-generation mergers with component masses in the mass gap may be especially enhanced in top-heavy GCs, motivating the existence of more GW190521-like mergers (Abbott et al. 2020a). In addition, the enhancement of collision rates and multiple-generation mergers in top-heavy GCs may also lead to the formation of IMBHs and even IMBH-IMBH mergers, as demonstrated in one of our models.

In general, we have shown that the high-mass slope of the cluster birth IMF may significantly impact the exact contribution to the cosmological BBH merger rate due to cluster dynamics. Specifically, if a large fraction of clusters were born with top-heavy IMFs, the cluster-dynamics merger rate may be somewhat enhanced relative to recent estimates (e.g., Kremer et al. 2020b). In turn, if a large fraction of clusters were born with top-light IMFs, the cluster-dynamics merger rate may be significantly reduced. With future observations of gravitational waves providing unique information on the BBH merger rate (Abbott et al. 2020b), it may be possible to leverage this understanding to better constrain the IMFs of old star clusters.

ORCID iDs

Newlin C. Weatherford ⓘ https://orcid.org/0000-0002-9660-9085
Giacomo Fragione ⓘ https://orcid.org/0000-0002-7330-027X
Kyle Kremer ⓘ https://orcid.org/0000-0002-4086-3180
Sourav Chatterjee ⓘ https://orcid.org/0000-0002-3680-2684
Claire S. Ye ⓘ https://orcid.org/0000-0001-9582-881X

---

[9] Just like the fictional Maw cluster (Anderson 1994), this "dark cluster" stage of a GC born with a top-heavy IMF may be short-lived due to the rapid pace of tidal evaporation.

Carl L. Rodriguez ⬤ https://orcid.org/0000-0003-4175-8881
Frederic A. Rasio ⬤ https://orcid.org/0000-0002-7132-418X

References

Abbott, R., Abbott, T. D., Abraham, S., et al. 2020a, PhRvL, 125, 101102
Abbott, R., Abbott, T. D., Abraham, S., et al. 2020b, arXiv:2010.14527
Adams, F. C., & Fatuzzo, M. 1996, ApJ, 464, 256
Adams, F. C., & Laughlin, G. 1996, ApJ, 468, 586
Anderson, K. J. 1994, Star Wars: The Jedi Academy Trilogy, Vol. 1, Jedi Search (New York: Bantam Spectra)
Askar, A., Szkudlarek, M., Gondek-Rosińska, D., Giersz, M., & Bulik, T. 2017, MNRAS, 464, L36
Astropy Collaboration, Robitaille, T. P., Tollerud, E. J., et al. 2013, A&A, 558, A33
Banerjee, S. 2017, MNRAS, 467, 524
Banerjee, S., & Kroupa, P. 2011, ApJL, 741, L12
Bartko, H., Martins, F., Trippe, S., et al. 2010, ApJ, 708, 834
Belczynski, K., Heger, A., Gladysz, W., et al. 2016, A&A, 594, A97
Bennett, C. L., Larson, D., Weiland, J. L., & Hinshaw, G. 2014, ApJ, 794, 135
Berti, E., Cardoso, V., Gonzalez, J. A., et al. 2007, PhRvD, 76, 064034
Breen, P. G., & Heggie, D. C. 2013, MNRAS, 432, 2779
Chatterjee, S., Fregeau, J. M., Umbreit, S., & Rasio, F. A. 2010, ApJ, 719, 915
Chatterjee, S., Rodriguez, C. L., & Rasio, F. A. 2017, ApJ, 834, 68
Chatterjee, S., Umbreit, S., Fregeau, J. M., & Rasio, F. A. 2013, MNRAS, 429, 2881
Chernoff, D. F., & Weinberg, M. D. 1990, ApJ, 351, 121
Clark, G. 1975, ApJ, 199, L143
Dabringhausen, J., Kroupa, P., & Baumgardt, H. 2009, MNRAS, 394, 1529
De Marchi, G., Panagia, N., & Beccari, G. 2017, ApJ, 846, 110
De Marchi, G., Paresce, F., & Pulone, L. 2007, ApJL, 656, L65
Dehnen, W., & Binney, J. 1998, MNRAS, 294, 429
Di Carlo, U. N., Mapelli, M., Bouffanais, Y., et al. 2020, MNRAS, 497, 1043
Downing, J. M. B., Benacquista, M. J., Giersz, M., & Spurzem, R. 2010, MNRAS, 407, 1946
Downing, J. M. B., Benacquista, M. J., Giersz, M., & Spurzem, R. 2011, MNRAS, 416, 133
Duquennoy, A., & Mayor, M. 1991, A&A, 500, 337
El-Badry, K., Quataert, E., Weisz, D. R., Choksi, N., & Boylan-Kolchin, M. 2019, MNRAS, 482, 4528
Fragione, G., & Banerjee, S. 2020, ApJL, 901, L16
Fragione, G., & Kocsis, B. 2018, PhRvL, 121, 161103
Fragione, G., Loeb, A., & Rasio, F. A. 2020a, ApJL, 895, L15
Fragione, G., Loeb, A., & Rasio, F. A. 2020b, ApJL, 902, L26
Fregeau, J. M., Gürkan, M. A., Joshi, K. J., & Rasio, F. A. 2003, ApJ, 593, 772
Giersz, M., Askar, A., Wang, L., et al. 2019, MNRAS, 487, 2412
Giesler, M., Clausen, D., & Ott, C. D. 2018, MNRAS, 477, 1853
González, E., Kremer, K., Chatterjee, S., et al. 2020, arXiv:2012.10497
Haghi, H., Khalaj, P., Hasani Zonoozi, A., & Kroupa, P. 2017, ApJ, 839, 60
Haghi, H., Safaei, G., Zonoozi, A. H., & Kroupa, P. 2020, ApJ, 904, 43
Harris, W. E., Morningstar, W., Gnedin, O. Y., et al. 2014, ApJ, 797, 128
Heggie, D., & Hut, P. 2003, The Gravitational Million-Body Problem: A Multidisciplinary Approach to Star Cluster Dynamics (Cambridge: Cambridge Univ. Press)
Heggie, D. C. 1975, MNRAS, 173, 729
Hénon, M. 1971a, Ap&SS, 13, 284
Hénon, M. 1971b, Ap&SS, 14, 151
Ivanova, N., Heinke, C. O., Rasio, F. A., Belczynski, K., & Fregeau, J. M. 2008, MNRAS, 386, 553
Joshi, K. J., Nave, C. P., & Rasio, F. A. 2001, ApJ, 550, 691
Joshi, K. J., Rasio, F. A., Zwart, S. P., & Portegies Zwart, S. 2000, ApJ, 540, 969
King, I. 1962, AJ, 67, 471
Kremer, K., Chatterjee, S., Rodriguez, C. L., & Rasio, F. A. 2018, ApJ, 852, 29
Kremer, K., Rodriguez, C. L., Amaro-Seoane, P., et al. 2019, PhRvD, 99, 063003
Kremer, K., Spera, M., Becker, D., et al. 2020c, ApJ, 903, 45
Kremer, K., Ye, C. S., Chatterjee, S., Rodriguez, C. L., & Rasio, F. A. 2020a, in IAU Symp. 351, Star Clusters: From the Milky Way to the Early Universe, ed. A. Bragaglia et al. (Cambridge: Cambridge Univ. Press), 357
Kremer, K., Ye, C. S., Rui, N. Z., et al. 2020b, ApJS, 247, 48
Kroupa, P. 2001, MNRAS, 322, 231
Lada, C. J., & Lada, E. A. 2003, ARA&A, 41, 57
Larson, R. B. 1998, MNRAS, 301, 569
Lousto, C. O., Campanelli, M., Zlochower, Y., & Nakano, H. 2010, CQGra, 27, 114006
Lyne, A., Brinklow, A., Middleditch, J., et al. 1987, Natur, 328, 399
Mackey, A. D., Wilkinson, M. I., Davies, M. B., & Gilmore, G. F. 2007, MNRAS, 379, L40
Mackey, A. D., Wilkinson, M. I., Davies, M. B., & Gilmore, G. F. 2008, MNRAS, 386, 65
Marks, M., Kroupa, P., Dabringhausen, J., & Pawlowski, M. S. 2012, MNRAS, 422, 2246
Morscher, M., Pattabiraman, B., Rodriguez, C., Rasio, F. A., & Umbreit, S. 2015, ApJ, 800, 9
Pattabiraman, B., Umbreit, S., Liao, W.-k., et al. 2013, ApJS, 204, 15
Rodriguez, C. L., Kremer, K., Grudić, M. Y., et al. 2020, ApJL, 896, L10
Rodriguez, C. L., Morscher, M., Pattabiraman, B., et al. 2015, PhRvL, 115, 051101
Rodriguez, C. L., Zevin, M., Amaro-Seoane, P., et al. 2019, PhRvD, 100, 043027
Sigurdsson, S., & Phinney, E. S. 1995, ApJS, 99, 609
Tichy, W., & Marronetti, P. 2008, PhRvD, 78, 081501
Verbunt, F., van Paradijs, J., & Elson, R. 1984, MNRAS, 210, 899
Wang, L. 2020, MNRAS, 491, 2413
Ye, C. S., Fong, W.-f., Kremer, K., et al. 2020, ApJL, 888, L10
Ye, C. S., Kremer, K., Chatterjee, S., Rodriguez, C. L., & Rasio, F. A. 2019, ApJ, 877, 122